Forecasting Critical Overloads based on Heterogeneous Smart Grid Simulation

Matthias Bittner[a], Daniel Hauer[b,d], Christian Stippel[d],
Katharina Scheucher[d] Robin Sudhoff[c], Axel Jantsch[a]
[a]Christian Doppler Laboratory for Embedded Machine Learning, TU Wien, Austria, {firstname.lastname}@tuwien.ac.at
[b]Siemens AG, Vienna, Austria, {firstname.lastname}@siemens.com
[c]Siemens AG, Erlangen, Germany, {lastname.firstname}@siemens.com
[d]TU Wien, Vienna, Austria, {firstname.lastname}@tuwien.ac.at

***Abstract*—Climate change mitigation poses a great challenge for our society. The need to reduce greenhouse gas emissions facilitates the expansion of renewable energy sources and electromobility. This transition is an already ongoing process, and with the worldwide increasing energy consumption, we face the need for automatic control and monitoring of the future electrical grid. To ensure a calculable and stable Low Voltage grid we need reliable load forecasting in order to avoid critical overloads and potential financial losses. This paper presents a novel concept for forecasting critical overloads based on an LSTM recurrent neural network. Our algorithm was tested using a one-year simulation of a rural Low Voltage grid section containing a grid-friendly energy community. Our results show the successful detection of 29 overloads within 12 simulated weeks. We reach a recall of 100% and a precision of 85%. Furthermore, we proved the ability of our LSTM to forecast two weeks with an MAE of 12.41 kW for the month of July. When optimizing the weather forecast data, we can lower this to 6.89 kW.**

***Index Terms*—Smart Grids, Load Forecasting, Energy Community, Simulation, Deep Learning**

I. Introduction

The effects of climate change are becoming more and more visible [1]. Reducing greenhouse gases requires strong efforts in changing our current lifestyle. The electrical grid, especially energy generation and the amount and way of consumption, will play a crucial role in climate change mitigation [2]. Tackling energy generation, renewable energy sources are one of the most affordable concepts for reducing the usage of fossil fuels and therefore restrict the CO_2 emissions [3]. However, renewable energy sources are characterized by their volatility and challenging predictability due to their dependence on external environmental factors. Besides these ongoing changes regarding energy generation sources, global energy consumption increases [4]. This is partly related to the electrification of mobility that serves the goal of CO_2 emission reduction [5].

The increasing variety in both energy generation and consumption poses great challenges for future electrical grids. Enhancing the resilience of Smart Grids, which essentially determines the amount of renewable energy that can be supplied to or sourced from the grid, is a crucial challenge [6]. The existing infrastructure will frequently be utilized to its maximum capacity. To avoid cost-intensive grid expansions, we experience a transition from passive grids to intelligent cyber-physical systems with different actuators in them ("Smart Grids"). The implementation of concepts like an Energy Community (EC) will optimize the usage of locally produced energy by controlling active components (e.g., electric vehicles, heating, ventilation, and air conditioning systems) and battery storages to increase local self-consumption [7]. Additionally, the operation of these new assets is influenced by factors such as irradiance, azimuth, and altitude of the sun [8], [9]. As different stakeholders such as ECs or Distribution System Operators (DSOs) may have conflicting goals (energy costs vs. grid stability), grid behavior becomes more incalculable and unstable. In combination with the closer operation to its borders, this raises the need for reliable monitoring and forecasting systems. A special focus has to be set on avoiding overloads in local grid sections, particularly Low Voltage (LV) grids. Knowing the future behavior and potential overloads allows for proactive interventions to avoid blackouts or cut-offs with financial losses.

Machine Learning (ML) approaches for time series forecasting are commonly used and subject to various applications in the literature (see Section II). Time series analysis for electricity systems can enable low-carbon electricity and reduce the climate impact of current systems [2]. Therefore, we propose a ML based forecasting approach to predict the load of LV grid sections with a focus on the prediction of overload situations. The main contributions of our work are:

- A medium-term forecasting algorithm for predicting critical grid load events based and evaluated on a simulated heterogeneous Smart Grid scenario.
- We provide a *heterogenous* Smart Grid benchmark dataset[1] for one year consisting of a rural LV grid section containing an optimized EC.

II. Related Work

A. Smart Grid Simulation

Smart Grid simulations serve as vital tools for comprehending and managing the complex dynamics of power grids. Several simulation platforms have been proposed, each offering different capabilities. CityLearn provides a Reinforcement Learning (RL) environment designed to model a microgrid

[1]Code and data accessible at: https://github.com/mbitob/forecasting-overloads-based-on-simulated-smartgrid-data

of nine buildings, incorporating various elements such as batteries, electric vehicles, water heaters, and photovoltaic panels [10]. Another framework, OPF-Learn, targets AC optimal power flow, providing tools for both Julia and Python [11]. It operates by uniformly sampling load profiles from a convex set that envelops the AC Optimal Power Flow (OPF) feasible set. PowerGridWorld, an open-source software package, creates multi-agent Gym environments for Smart Grid simulations [12]. It allows multiple actors to influence the grid simultaneously, a feature that becomes crucial as the complexity of the grid grows, and centralized control approaches become infeasible. Another contribution is BeoBench, a Python toolkit that offers unified access to existing building simulations from multiple frameworks [13]. This toolkit comprises several distinct building models in frameworks such as BOPTEST with three residential and commercial buildings [14], Energym with six residential, commercial, and office buildings [15], RL Testbed with one data center building [16], and Sinergym with three buildings including a data center, a residential building, and an office [17]. While these platforms offer a wide range of simulation capabilities, they are not applicable to fully represent interactions of new stakeholders (e.g., ECs, DSOs) within a rural LV grid, underscoring the need for more comprehensive and adaptable simulation environments.

B. Smart Grid Datasets

Datasets play a critical role in advancing research, especially in the field of Smart Grids. However, obtaining access to real-world data for critical infrastructures can be challenging, particularly for security research purposes. The work of Ahmed et al. addresses this issue by collecting and sharing a comprehensive dataset from a real-world Smart Grid testbed, thus making a significant contribution to the research community [18]. Another notable approach comes from Arzamasov et al., who propose Decentral Smart Grid Control (DSGC) as a system to implement demand response without requiring significant changes to the infrastructure [19]. Through data-mining techniques, the authors aim to remove simplifications common in DSGC models, such as the assumption of identical behavior among all grid participants. Using many simulations with diverse input values and applying decision trees to the resulting data, they gain new insights into the system, discovering, for instance, that the system can remain stable even if some participants adapt their energy consumption with a high delay. Despite the valuable insights these datasets provide, there is a need for more diversified and representative datasets to reflect the heterogeneity and dynamic behavior inherent to new stakeholders within rural LV grids.

C. Load Forecasting and Event Detection in Smart Grids

Predicting load patterns and detecting events in Smart Grids are essential to ensure the grid's stability and efficiency. Load forecasting approaches can be categorized based on the forecasting horizon, including Short-Term Load Forecasting (STLF), Medium-Term Load Forecasting (MTLF), and Long-Term Load Forecasting (LTLF) [20]. Existing techniques for forecasting and event detection include advanced machine learning models such as Long Short-Term Memory (LSTM) and Generative Adversarial Networks (GANs) [21]–[23], as well as hybrid algorithms explicitly designed for event detection, localization, and classification in power systems [24]. However, existing work lacks the capability to forecast safety critical loads based on future-proof heterogeneous Smart Grid simulation scenarios.

III. Methodology

A. Heterogeneous Smart Grid Simulation

We introduce a Smart Grid simulation environment of a local Renewable Energy Community (REC) based on the work from [25]. This existing environment will serve as a virtual testbed for data generation for this work, as it includes various actors, resulting in a reliable and future-proof setup.

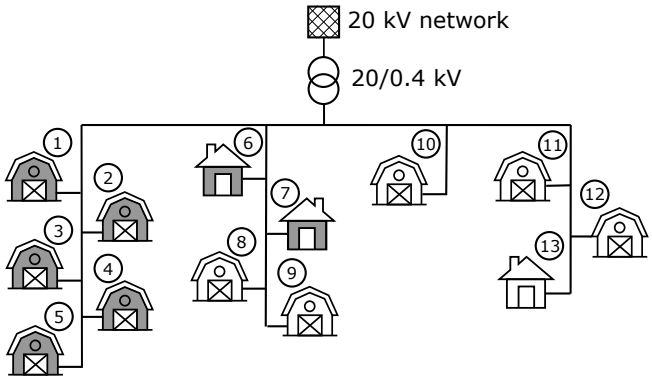

Fig. 1: Topology of the simulated rural LV grid with its four feeders and 13 buildings. 7 of them are part of the REC (grey) and 6 not (white).

The simulation use case represents a typical rural LV grid in which a REC performs grid-friendly operations characterized by minimizing electricity costs for all participants while complying with DSO constraints. All design parameters were taken from the SimBench dataset *"LV-rural1"* [26] for a future scenario of the year 2034 with the extensive deployment of Photovoltaic (PV) systems and batteries. This includes the topology, dimensioning of the transformer, PV systems, household batteries, and Electric Vehicle (EV) charging stations as well as the electric household load profiles. Table I gives an overview of the different assets and the selected 50% REC participants and Fig. 1 sketches the grid topology. The simulated LV grid section is connected to the medium voltage grid by one transformer (distribution substation). The substation, with a capacity of 250 kVA, is designed to be operated at 80% of its rated power, hence 200 kW. Transformer overloads are power dips above (for demand) or below (for feed-in) this threshold.

The framework for our Smart Grid simulation, as shown in Fig. 2, is composed of three software components communicating via application programming interfaces (REST APIs).

The "BIFROST Virtual Testbed" models the behavior of the LV grid section. BIFROST is a co-simulation framework that consists of a discrete core simulation engine and a 3D web UI

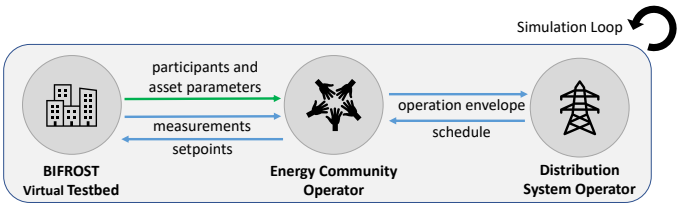

Fig. 2: Simulation framework overview

for the use case creation [27]. The core provides an editable data model for external simulation models, which have to register at the core using a REST API. In every discrete simulation step, BIFROST calls the connected modules and they can respond with new simulation data (e.g., new household load or new outdoor temperature). All values are stored in an influx database and can be visualized using the BIFROST UI. Fig. 3 shows a screenshot of the simulated rural grid section. In the given simulation environment, BIFROST uses a load-flow solver, a weather generation module as well as a model for all buildings, including PV systems, household batteries, and EV charging stations. The building model includes the logic for both REC participants and households that are not part of the REC, which are referred to as non-participants. While the existing profiles for all passive assets (i.e. household base loads) are directly used from the SimBench data set, all active assets (i.e. PV systems, batteries, and EV charging slots) are modeled by BIFROST and only the dimensioning parameters, e.g., the installed PV power and size of batteries, are taken from SimBench. The PV generation is derived based on weather data from Vienna in 2021 [28]. Weather Forecast data is based on corresponding historic data from [29]. The behavior of the batteries and EV charging slots is simulated using state of the art physical models.

The Energy Community Operator (ECO) optimizes the flexibility deployment of REC participants' controllable assets to optimize the collective REC operation [30]. In every simulation step, the building model forwards all current measurements to the ECO. The ECO uses measurement data of the last week and day-ahead weather forecasts to perform a cost-optimization of the REC. A linear optimization is addressed, wherein decision variables include the power for charging and

TABLE I: Composition of the simulated rural LV settlement and the REC members.

complete LV grid section	
13 participants	3 households, 10 farms
13 PV systems	520 kWp
5 battery storages	421 kWh
5 EV charging stations	2×3.7 kW, 2×11 kW, 1×22 kW
REC participants	
7 participants	2 households, 5 farms
7 PV systems	285 kWp
3 battery storages	245 kWh
4 EV charging stations	1×3.7 kW, 2×11 kW, 1×22 kW

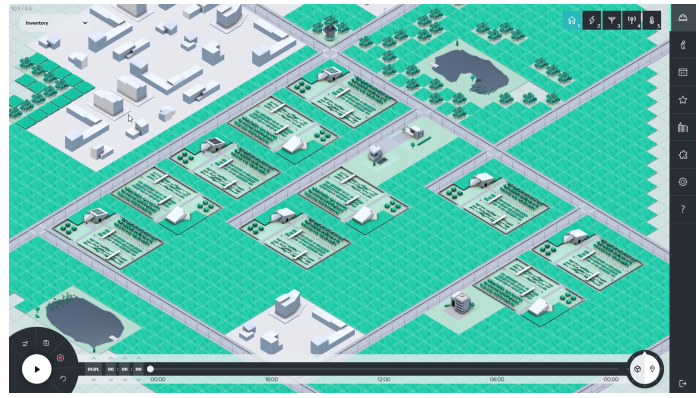

Fig. 3: Low-Voltage (LV) grid section in the BIFROST UI with different agricultural and residential buildings.

discharging of batteries, curtailment of PV systems, and the charging power allocation of EV charging stations. Resulting variable values, referred to as setpoints, are sent back to the building model, which implements them and changes the operation of the assets accordingly. As the ECO focuses on optimal utilization of renewable generated energy within the REC to minimize its costs, this can cause a response that might lead to overloads for both infeed and demand at the local distribution substation.

Therefore, the ECO communicates its scheduled behavior to the DSO. The DSO then calculates time-dynamic active power demand and feed-in limits, called "operating envelope" (OE), which is communicated to the ECO. The OE represents a virtual boundary for the REC's total residual load, which is then used as a constraint in the optimization problem. The calculation of the OE is based on the substation transformer's rated power capacity and a naive forecast for the non-participants' load.

While the overall goal of this setup is the avoidance of transformer overloads, this can not always be guaranteed. The monitored limit violations can be caused by:

- **Physical limitations**: Batteries can not always be charged or discharged as required, e.g., due to state of charge or power limitations.
- **Deviating weather forecast data**: The ECO uses weather forecast data for its operation scheduling. The forecast data is prone to differ from the real weather measurements due to forecast uncertainties.
- **Deviating human behavior forecast**: Both the ECO and the DSO forecast load related to human behavior, e.g., for calculation of the OE, which is subject to uncertainties. Hence, household load or utilization of EV charging stations might differ.

We, therefore, propose a monitoring concept, which is independent of the Smart Grid actors such as ECO and DSO in the simulation setup. The concept enables the prediction of critical loads, specifically the residual load at the distribution substation, by forecasting daily load profiles.

B. Grid Load Forecasting

Recurrent Neural Networks (RNNs) are widely used for load forecasting in electrical Smart Grids [31]. The crucial part for successful training is the proper definition of the lookback window L, which specifies the amount of information allowed to be *seen* by the network before predicting a new value. The nature of the different features used for training also has a huge impact on the forecasting performance (Section IV-C). Once a proper lookback window L and useful features such as weather, sun position, and temperature are fixed and the network is trained, one is able to perform forecasting.

Short-term forecasting for a single time point can be achieved solely on historical data. If it is desired to forecast for a longer period, such as a whole day, it is achieved in an autoregressive fashion. Besides the autoregressive forecasting of the active power, one also needs additional features for the to-be-predicted time points. This future feature information can either be generated through mathematical models, e.g., an astronomical model for the sun's position, adding the missing features as an additional forecasting feature, or using weather forecast data such as solar radiation. Fig. 4 provides a structural overview for the autoregressive medium-term load forecasting used in our approach.

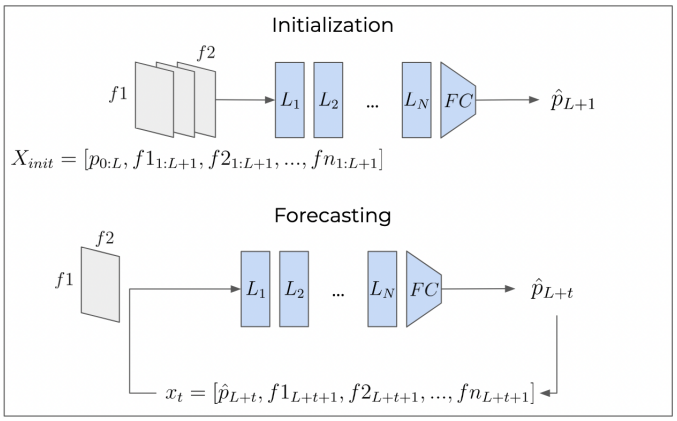

Fig. 4: Reccurrent autoregressive Load-Forecasting. Firstly, the RNN and its hidden cell states are initialized with original historical feature values with a lookback sequence length of L. Then $\hat{p}$ is forecasted in an autoregressive fashion until we reach the end of the forecasting window $t = T$.

IV. Experimental Results

We evaluate our proposed methodology by simulating a settlement consisting of an EC with an equal amount of participants and non-participants. This simulated heterogeneous data (Section IV-A) is used to train a LSTM for load forecasting (Section IV-B). We show the mid-term forecasting performance (Section IV-C) and the accuracy for detecting safety-critical load events (Section IV-D) on a monthly basis.

A. Heterogeneous Dataset

Based on the setup described in Section III-A we introduce a high-resolution dataset to explore the dynamic interactions within an EC. The dataset is derived from a simulation covering a one-year period that captures the complexity of system dynamics, including load demand variations, solar power production, and the effects of environmental factors. The main features used from the simulation are:

- **Time t:** Simulation time with a resolution of 15 minutes.
- **Active Power p:** Active Power at the transformer in kW.
- **Sun Altitude θ:** The angle relative to the horizon.
- **Sun Azimuth ϕ:** The compass direction of the sun.
- **Actual Solar Irradiance ζ:** Measured in $\mathrm{W/m^2}$.
- **Forecasted Solar Irradiance $\hat{\zeta}$**

Active power and irradiance readings provide insight into the grid's energy consumption and generation patterns. Simultaneously, solar altitude and azimuth data are crucial for determining the efficiency of solar power generation and serve as positional encoding for the machine learning models.

Fig. 5 provides a detailed view of two exemplary days from the simulated dataset and displays the dataset of the full year, delineating the division into training, validation, and test sets.

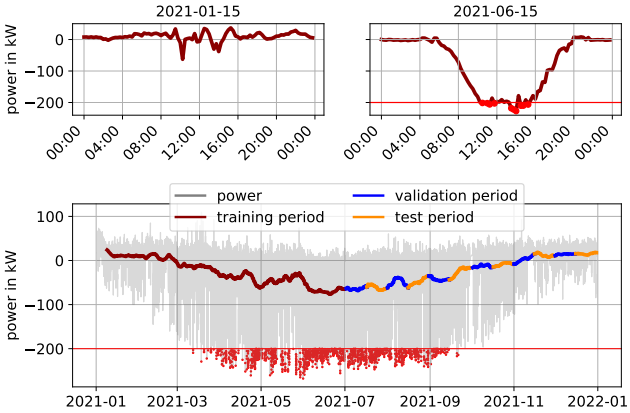

Fig. 5: Top: Two selected days showing power demand and generation variations on January 15th and June 15th.
Bottom: Entire dataset demonstrating the division into training, validation, and test sets. Smoothing is achieved with a rolling mean over four weeks. Negative values represent infeed.

The first subplot on the top left illustrates a day in winter, specifically chosen from January, showing relatively low solar power generation and therefore no overload. The second subplot on the top right illustrates a day in summer, chosen from June, where the active power dips below -200 kW due to excess power production. The bottom subplot shows the smoothed active power over a year as well as the overloads. It clearly shows that there is a seasonal trend that is mirrored around June. The data for the first six months is used for training (dark red). To keep seasonal effects in validation (blue), and testing (orange) we divide the rest into 15 days sections.

B. Neural-Architecture and Training

RNNs and especially LSTMs are well suited to handle and process sequential data. Their internal long short-term

memory cell and the recurrent structure are known to be effective, for time series forecasting applications [32]. The Neural Network (NN) architecture used for our experiments consists of four LSTM cells with a hidden size of 50, followed by a single fully connected layer that maps the 50 hidden states of the last layer to a scalar prediction output. All experiments are implemented with PyTorch We train the network for 100 epochs and use the standard Adam optimizer [33] with $\beta_1 = 0.9, \beta_2 = 0.999, \epsilon = 10^{-8}$. Cosine annealing with warm restarts [34], an initial learning rate of 10^{-3} and a period of $T_0 = 10$ is used as a learning rate scheduler. Additionally, we use a batch size of 64 and Mean Squared Error (MSE) as a loss function. We train on a single Tesla V100S-PCIE-32GB. The best network is stored based on the checkpoint with the lowest validation loss.

The effects and influences of using and combining different input features for forecasting the active power p are analyzed with three experiments (Table II). The scenario of using the historic active power, sun position, and the original irradiance during training results in the lowest validation loss. All experiments, including the forecasting accuracy on the test set, are discussed in more depth in Section IV-C.

TABLE II: Input features, experiment names, minimum validation loss during training, Multiply–Accumulates (MACs) for predicting a single time step, and the number of parameters of the model when training with different input features.

NN input features	experiment name	validation loss	MACs	params
$x = [p]$	no metadata	17.68×10^{-4}	146.85k	71.85k
$\mathbf{x} = [p, \theta, \phi]$	sun position	16.55×10^{-4}	147.65k	72.25k
$\mathbf{x} = [p, \theta, \phi, \zeta]$	sun position + orig. irradiance	6.71×10^{-4}	148.05k	72.45k

During training, we consider the proposed train and validation splits (Section IV-A) for updating and evaluating the network. Sequence datasets are generated for the training and validation splits. One sequence feature and label pair,

$$\mathbf{X}_i = [\mathbf{p}_{i:i+L}, \boldsymbol{\theta}_{i+1:i+L+1}, \boldsymbol{\phi}_{i:i+L+1}, \boldsymbol{\zeta}_{i+1:i+L+1}], \quad (1)$$

$$y_i = p_{i+L+1}, \quad (2)$$

consists of the features $\mathbf{X}_i \in \mathbb{R}^{4\times L}$, and label $y_i \in \mathbb{R}^1$. Each element *i* in the test and validation sequence dataset is corresponding to a sliding window generated with a stride of one and a lookback window of $L = 100$. With a 15-minute resolution, this corresponds to a lookback window of 25 hours.

C. Grid Load Forecasting

To show the importance of the different input features, we compare the resulting grid load forecasts based on the test set for the individual months for each of the three trained models and scenarios (Table II). We generate forecasts for a whole day, by initializing the LSTM and its hidden states with the original measurements of a whole previous day. Then we forecast the power consumption $\hat{\mathbf{p}} \in \mathbb{R}^{1\times96}$ for the whole future day in an autoregressive fashion (details Fig. 4). The test set for each month consists of 15 days. Since the previous day is always exploited for initialization we are able to generate forecasts for 14 days, which results in $\hat{\mathbf{P}}_{month} \in \mathbb{R}^{14\times96}$ for each month and scenario.

Fig. 6 visualizes the results including their daily mean power profiles and standard deviation $\overline{\mathbf{p}} \pm \sigma_{\overline{\mathbf{p}}}$ for the different months and different input features. In the following, we explain the results of each experiment in more depth.

***Test Set*:** The true distribution for the daily power profiles of the test set for each month is visualized in green (Fig. 6). The mean is highlighted with a solid line. The standard deviation is indicated by the area plot.

***No Meta Data*:** The first experiment of forecasting the active power just by considering the historic power as an input feature $\mathbf{x} = [\hat{p}]$ is visualized in red (Fig. 6). We observe that the network is not able to forecast the real amplitude and does not resolve the seasonal effects. Additionally, we face the issue of a phase shift due to the lack of a positional encoding.

***Sun Position*:** The sun's position is based on an astronomical model and can be calculated at any time and at any geological position. Including the sun's position to the feature vector $\mathbf{x} = [\hat{p}, \theta, \phi]$ enables the capability to encode positional information on a local (daily) scale due to the azimuth ϕ and the sinusoidal amplitude of the altitude θ. The seasonal effects are encoded due to the offset shift of the altitude. This hypothesis is confirmed, by investigating the graphs in blue (Fig. 6). It is clearly visible, that we avoid the phase shift, that the expected daily mean profiles are similar to the test set ones, and that the seasonal descending amplitude from July to December is covered. The only drawback left is the low variance due to the missing irradiance information.

***Sun Position & Irradiance Forecasts*:** For this experiment (Fig. 6, depicted in yellow), we train the network with the original irradiance ξ. The evaluation is based on the feature vector $\mathbf{x} = [\hat{p}, \theta, \phi, \hat{\xi}]$ with the forcasted irradiance. Again, we have no phase shift, and the expected values match the test set ones. The standard deviation increases compared to the scenario of not including the irradiance in the feature vector. Comparing the green area, associated with the variance of the real test data, and the yellow area, corresponding to the variance for the predictions when using solar irradiance forecasts, we still observe a lower variance. The higher variance in the test set is caused by fluctuations of the real irradiance, due to spontaneous cloud coverage. Such effects are rather unpredictable and not covered, by our irradiance forecasts.

Next, we showcase the forecasting performance difference between using the original irradiance vs irradiance forecasts. To simulate an ideal weather forecast we replace $\mathbf{x} = [\hat{p}, \theta, \phi, \hat{\xi}]$ by $\mathbf{x} = [\hat{p}, \theta, \phi, \xi]$. We compare the Mean Absolute Error (MAE) and Root Mean Squared Error (RMSE) errors for both scenarios on a monthly basis (Fig. 7). We observe the effect, that the prediction error is always higher when using the irradiance forecasts, especially in the summer months (July, August, and September). This is due to a higher impact of the discrepancy between the forecasted and real irradiance and its direct impact on the PV-systems production.

The error in August is the highest since the forecasts are deviating stronger compared to July and September. We also note that the difference between the two errors is decreasing with the declining impact of the PV systems, caused due to the seasonal effect of the sun's altitudes θ offset.

To analyze the forecasting error on a more fine-grained level we provide the forecasting results for the whole test set of July (Fig. 8). The upper half of the graph shows the original active power time series and the generated power predictions when using the irradiance forecasts. The lower plot compares the absolute error for using original irradiance vs irradiance forecasts. The difference in the error is higher at the active power dips caused by unpredictable cloud coverage. The still remaining error when comparing the ground truth and the prediction with the original irradiance can be interpreted as the model error caused by different consumption patterns, deviating from the training/validation data.

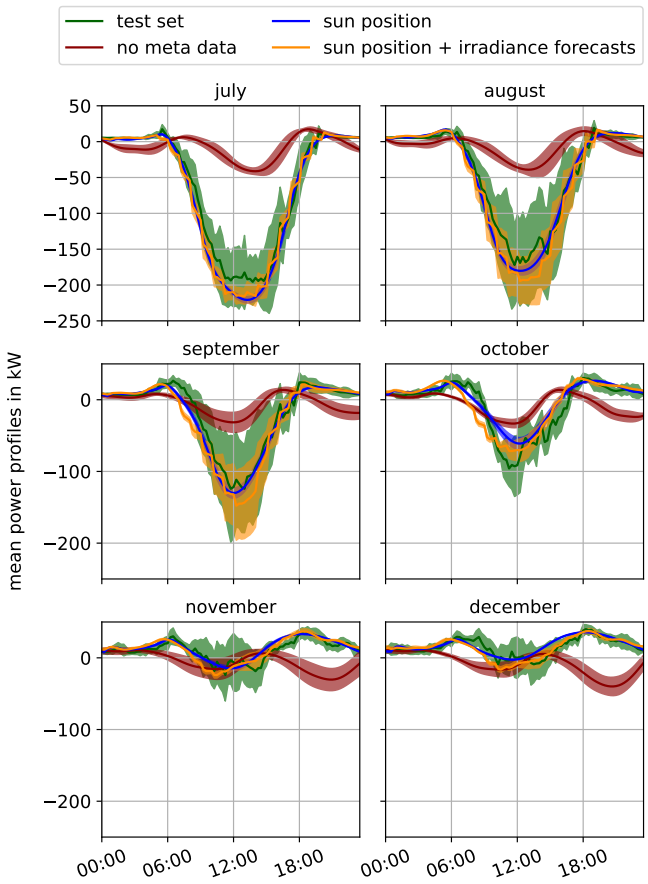

Fig. 6: The comparison of the daily mean power profile $\overline{p} \pm \sigma_{\overline{p}}$ of the ground-truth in the test set and the resulting forecasts. The results for the three trained networks show the effect of the individual heterogeneous features on a monthly basis.

D. Grid-Overload detection

Our simulation study covers a smart grid scenario with an existing EC consisting of participants known to the ECO and participants not fully considered during optimization (Table I).

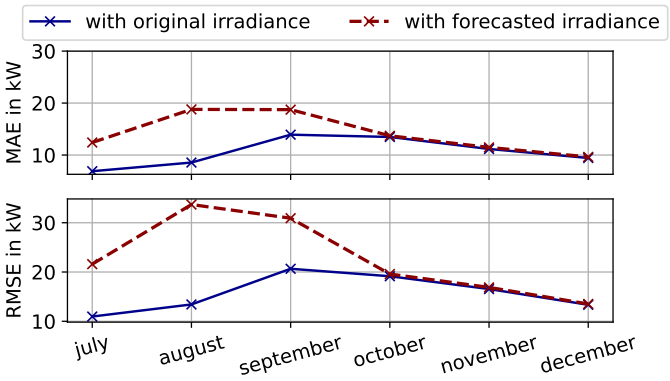

Fig. 7: MAE and RMSE for medium-term forecasts on a monthly basis. We initialize with the first day and forecast for the remaining 14 days of the test set. We compare the real-world scenario of using irradiance forecasts vs the original irradiance in order to highlight the drawback of unpredictable variations in real weather data.

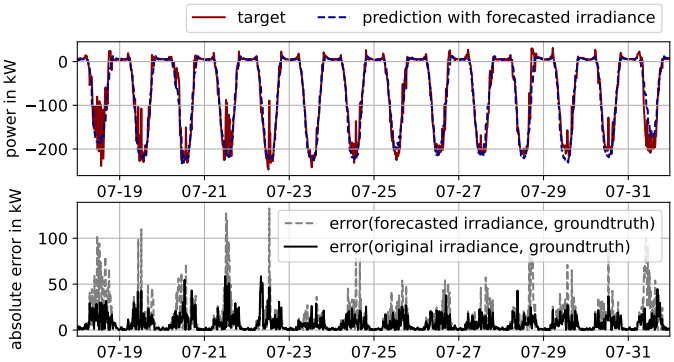

Fig. 8: Medium-term forecasting for the test set in July. We initialize the hidden states of the LSTM with the first day and forecast for the remaining 14 days. We highlight the non-preventable error due to the difference between the original irradiance and its forecast.

This discrepancy can lead to scenarios where we face power dips below -200 kW (feed-in limit). With our approach, we are able to forecast and detect these so-called critical transformer overloads. Detecting these events a day in advance can help the system operator (e.g., ECO or DSO) take action before overloads occur.

For this specific experiment, we consider the real-world scenario of using the forecasting model with the sun position and irradiance forecasts as input features $\mathbf{x} = [\hat{p}, \theta, \phi, \hat{\xi}]$. Forecasts are again generated for a whole day, by initializing the LSTM and its hidden states with the original historic measurements of a whole previous day. If the forecasted power consumption $\hat{\mathbf{p}} \in \mathbb{R}^{1\times 96}$ for the whole future day hurts the feed-in limit of -200 kW once, we mark the day as *positive* detected grid overload. The overall performance compared to the original ground truth of the test set is again evaluated on a monthly basis and depicted in Table III.

TABLE III: Overload detection results for a feed-in limit of -200 kW. Once setting the detection threshold to the feed-in limit and once to -159 kW. We analyze the amount of *true-positives* (TP), *true-negatives* (TN), *false-positives* (FP), and *false-negatives* (FN). In each column, we give $\mathrm{No}_{-200\ \mathrm{kW}}/\mathrm{No}_{-159\ \mathrm{kW}}$, corresponding to the number of occurrences with respect to the respective threshold.

month	TP	TN	FP	FN	acc	f1
july	12 / 14	0 / 0	0 / 0	2 / 0	0.86/1.00	0.92/1.00
august	8 / 13	1 / 1	0 / 0	5 / 0	0.64/1.00	0.76/1.00
september	0 / 2	11 / 7	1 / 5	2 / 0	0.79/0.64	- /0.44
october	0 / 0	14 / 14	0 / 0	0 / 0	1.00/1.00	-
november	0 / 0	14 / 14	0 / 0	0 / 0	1.00/1.00	-
december	0 / 0	14 / 14	0 / 0	0 / 0	1.00/1.00	-

Taking a recap on the year-long simulated active power profile (Fig. 5), we observe that the critical overloads are mostly occurring during the summer months (April-September). This is also reflected in the detection results, by e.g., correctly identifying all days as *true-negatives* in October-December. The highest interest, from theDSOs's perspective, remains in correctly identifying *true-positives* and minimizing the amount of *false-negatives*. To analyze this behavior in more depth, we compare the *area-of-harm* and *time-of-harm*,

$$E_{\mathrm{harm}} = \sum_{\substack{i \\ |p_i| \geq 200\ \mathrm{kW}}} (|p_i| - 200\ \mathrm{kW}) T_{\mathrm{sample}} \tag{3}$$

$$T_{\mathrm{harm}} = \sum_{\substack{i \\ |p_i| \geq 200\ \mathrm{kW}}} T_{\mathrm{sample}}, \tag{4}$$

which indicates the amount of energy E_{harm}, and the time period T_{harm} of the transformer facing an overload based on the sample time $T_{\mathrm{sample}} = 15\mathrm{min}$.

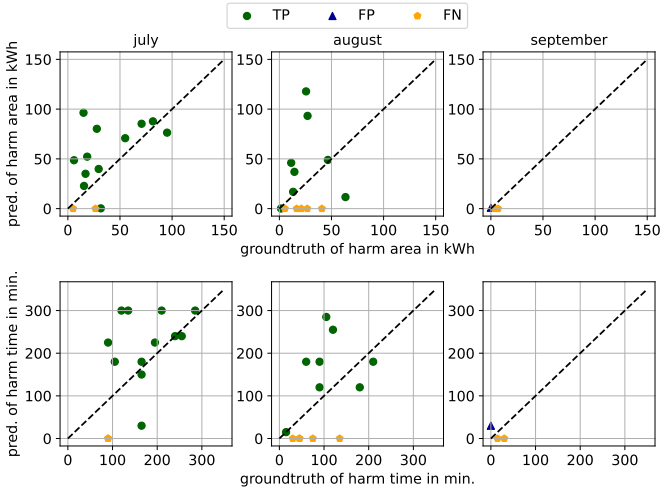

Fig. 9: Comparison of *area-of-harm* and *time-of-harm* between the ground-truth and the predictions.

Fig. 9 compares the *area-of-harm* and *time-of-harm* between the ground-truth and the predictions. Analyzing the critical and unwanted *false-negatives* we note that these are edge cases (low E_{harm} and T_{harm}), caused by real irradiance outlier, not covered by our forecasts. Modifying and lowering the active power threshold used for detecting overloads can reduce the amount of *false-negatives*. E.g., setting the threshold to -159 kW results in no *false-negatives* and four additional *false-positives* (Table III).

V. Conclusion and Outlook

We demonstrated a novel approach for forecasting critical overloads in a Smart Grid simulation scenario. Our algorithm is based on a lightweight LSTM recurrent neural network, with $72.45k$ parameters and $148.05k$ MACs, corresponding to 283kB in storage and 12.3ms latency for a single time-step forecast on a NUCLEO-L432KC - ARM Cortex M4 (assuming 4 Bytes per parameter and $\approx$ 12M MACs/s). It is able to provide medium-term forecasts for the load at a LV transformer. The network is trained using simulated load data of a transformer, the sun's altitude and azimuth, and irradiance data. During the forecasting step, we use the sun position and irradiance from weather forecast data to calculate the future transformer load. In particular, the algorithm is used to predict overloads at the transformer on a day-ahead base.

We verified our approach with a one-year simulation of a rural LV grid based on realistic data from the SimBench data set [26] and a grid-friendly EC according to [30] and [25]. The LSTM is trained using data from January to June and verified using 12 weeks in the time period from July to December, encompassing the seasonal cycle (winter to summer) for both training and validation. In the evaluated test set (opposite 12 weeks in the second half of the year) our algorithm was able to detect 20 out of 29 overloads resulting in a precision of 95% and a recall of 69%. As missed alerts (FN) are more system critical but at the same time often based on short and minor load exceedances, we also showed that lowering the alerting threshold for the prediction can increase the recall to 100% while keeping the precision at 85%. In addition, we proved the ability of our algorithm to forecast two weeks with an MAE of 12.41 kW in July. As renewable energy sources such as PV systems heavily rely on weather data, we could also show that enhancing the quality of weather forecasts improves prediction accuracy. With an optimal irradiance forecast the MAE can be reduced to 6.89 kW in our two-week prediction for July.

While this work already tackles multiple influential aspects of Smart Grids such as seasonal behavior and the coexistence of multiple active stakeholders, additional simulations and real-world experiments could further prove the validity of our LSTM-based forecasting algorithm. Including other topologies (e.g., from the SimBench data set) could be used to show and optimize the algorithm's independence of the system's structure and components. Further studies should also consider the neural network implementation on edge devices and incorporating other relevant domains for the Smart Grid (e.g., heat pumps, wind turbines, etc.) which could show the need for additional features such as temperature or wind data.

ACKNOWLEDGMENTS

This work is supported by the Austrian Federal Ministry for Digital and Economic Affairs, the National Foundation for Research, Technology, and Development, the Christian Doppler Research Association, by the FFG SENSE project (Nr FO999894802) and the AI-flex project. AI-flex (Nr 898486) has received funding in the framework of the joint programming initiative ERA-Net Smart Energy Systems' focus initiative Digital Transformation for the Energy Transition, with support from the European Union's Horizon 2020 research and innovation program under grant agreement No 883973.

REFERENCES

[1] M. Almazroui, F. Saeed, S. Saeed, M. Ismail, M. A. Ehsan, M. N. Islam, M. A. Abid, E. O'Brien, S. Kamil, I. U. Rashid *et al.*, "Projected changes in climate extremes using cmip6 simulations over srex regions," *Earth Systems and Environment*, vol. 5, no. 3, pp. 481–497, 2021.

[2] D. Rolnick, P. L. Donti, L. H. Kaack, K. Kochanski, A. Lacoste, K. Sankaran, A. S. Ross, N. Milojevic-Dupont, N. Jaques, A. Waldman-Brown *et al.*, "Tackling climate change with machine learning," *ACM Comput. Surv.*, vol. 55, no. 2, pp. 42:1–42:96, 2023. [Online]. Available: https://doi.org/10.1145/3485128

[3] A. Olabi and M. A. Abdelkareem, "Renewable energy and climate change," *Renewable and Sustainable Energy Reviews*, vol. 158, p. 112111, 2022.

[4] "World energy and climate statistics – yearbook 2023," https://yearbook.enerdata.net/, accessed: 2023-07-11.

[5] C. Thiel, W. Nijs, S. Simoes, J. Schmidt, A. van Zyl, and E. Schmid, "The impact of the eu car co2 regulation on the energy system and the role of electro-mobility to achieve transport decarbonisation," *Energy Policy*, vol. 96, pp. 153–166, 2016.

[6] L. Das, S. Munikoti, B. Natarajan, and B. Srinivasan, "Measuring smart grid resilience: Methods, challenges and opportunities," *Renewable and Sustainable Energy Reviews*, vol. 130, p. 109918, 2020.

[7] T. Leopold, V. Bauer, A. Brathukin, D. Hauer, S. Wilker, G. Franzl, R. Mosshamrner, and T. Sauter, "Simulation-based methodology for optimizing energy community controllers," in *2021 IEEE 30th International Symposium on Industrial Electronics (ISIE)*, 2021, pp. 1–6.

[8] C. Lamnatou, D. Chemisana, and C. Cristofari, "Smart grids and smart technologies in relation to photovoltaics, storage systems, buildings and the environment," *Renewable Energy*, vol. 185, pp. 1376–1391, 2022.

[9] O. M. Butt, M. Zulqarnain, and T. M. Butt, "Recent advancement in smart grid technology: Future prospects in the electrical power network," *Ain Shams Engineering Journal*, vol. 12, no. 1, pp. 687–695, 2021.

[10] J. R. Vázquez-Canteli, J. Kämpf, G. Henze, and Z. Nagy, "Citylearn v1. 0: An openai gym environment for demand response with deep reinforcement learning," in *Proceedings of the 6th ACM International Conference on Systems for Energy-Efficient Buildings, Cities, and Transportation*, 2019, pp. 356–357.

[11] T. Joswig-Jones, K. Baker, and A. S. Zamzam, "Opf-learn: An open-source framework for creating representative ac optimal power flow datasets," in *2022 IEEE Power & Energy Society Innovative Smart Grid Technologies Conference (ISGT)*. IEEE, 2022, pp. 1–5.

[12] D. Biagioni, X. Zhang, D. Wald, D. Vaidhynathan, R. Chintala, J. King, and A. S. Zamzam, "Powergridworld: A framework for multi-agent reinforcement learning in power systems," in *Proceedings of the Thirteenth ACM International Conference on Future Energy Systems*, 2022, pp. 565–570.

[13] A. Findeis, F. Kazhamiaka, S. Jeen, and S. Keshav, "Beobench: a toolkit for unified access to building simulations for reinforcement learning," in *Proceedings of the Thirteenth ACM International Conference on Future Energy Systems*, 2022, pp. 374–382.

[14] D. Blum, J. Arroyo, S. Huang, J. Drgoňa, F. Jorissen, H. T. Walnum, Y. Chen, K. Benne, D. Vrabie, M. Wetter *et al.*, "Building optimization testing framework (boptest) for simulation-based benchmarking of control strategies in buildings," *Journal of Building Performance Simulation*, vol. 14, no. 5, pp. 586–610, 2021.

[15] P. Scharnhorst, B. Schubnel, C. Fernández Bandera, J. Salom, P. Taddeo, M. Boegli, T. Gorecki, Y. Stauffer, A. Peppas, and C. Politi, "Energym: A building model library for controller benchmarking," *Applied Sciences*, vol. 11, no. 8, p. 3518, 2021.

[16] T. Moriyama, G. De Magistris, M. Tatsubori, T.-H. Pham, A. Munawar, and R. Tachibana, "Reinforcement learning testbed for power-consumption optimization," in *Methods and Applications for Modeling and Simulation of Complex Systems: 18th Asia Simulation Conference, AsiaSim 2018, Kyoto, Japan, October 27–29, 2018, Proceedings 18*. Springer, 2018, pp. 45–59.

[17] J. Jiménez-Raboso, A. Campoy-Nieves, A. Manjavacas-Lucas, J. Gómez-Romero, and M. Molina-Solana, "Sinergym: a building simulation and control framework for training reinforcement learning agents," in *Proceedings of the 8th ACM International Conference on Systems for Energy-Efficient Buildings, Cities, and Transportation*, 2021, pp. 319–323.

[18] C. M. Ahmed and N. K. Kandasamy, "A comprehensive dataset from a smart grid testbed for machine learning based cps security research," in *Cyber-Physical Security for Critical Infrastructures Protection: First International Workshop, CPS4CIP 2020, Guildford, UK, September 18, 2020, Revised Selected Papers 1*. Springer, 2021, pp. 123–135.

[19] V. Arzamasov, K. Böhm, and P. Jochem, "Towards concise models of grid stability," in *2018 IEEE international conference on communications, control, and computing technologies for smart grids (SmartGridComm)*. IEEE, 2018, pp. 1–6.

[20] H. Habbak, M. Mahmoud, K. Metwally, M. M. Fouda, and M. I. Ibrahem, "Load forecasting techniques and their applications in smart grids," *Energies*, vol. 16, no. 3, 2023. [Online]. Available: https://www.mdpi.com/1996-1073/16/3/1480

[21] M. Alazab, S. Khan, S. S. R. Krishnan, Q.-V. Pham, M. P. K. Reddy, and T. R. Gadekallu, "A multidirectional lstm model for predicting the stability of a smart grid," *IEEE Access*, vol. 8, pp. 85 454–85 463, 2020.

[22] A. Aligholian, A. Shahsavari, E. M. Stewart, E. Cortez, and H. Mohsenian-Rad, "Unsupervised event detection, clustering, and use case exposition in micro-pmu measurements," *IEEE Transactions on Smart Grid*, vol. 12, no. 4, pp. 3624–3636, 2021.

[23] D. Hauer, M. Bittner, S. Cejka, R. Mosshammer, F. Kintzler, T. Leopold, and S. Wilker, "Re-enacting rare multi-modal real-world grid events to generate ml training data sets," in *2021 IEEE 30th International Symposium on Industrial Electronics (ISIE)*, 2021, pp. 01–06.

[24] A. Anshuman, B. K. Panigrahi, and M. K. Jena, "A novel hybrid algorithm for event detection, localisation and classification," in *2021 9th IEEE International Conference on Power Systems (ICPS)*. IEEE, 2021, pp. 1–6.

[25] J. Kainz, R. Sudhoff, G. Engelbrecht, A. Einfalt, I. Fohler, D. Hauer, C. Kahler, R. Liedy, D. Menz, S. Schreck, A. Schuster, and S. Thiem, "Grid-friendly renewable energy communities using operating envelopes provided by dsos," in *CIRED 2023 - 27th International Conference on Electricity Distribution*, no. 11051. IET, 2023.

[26] S. Meinecke, D. Sarajlić, S. R. Drauz, A. Klettke, L.-P. Lauven, C. Rehtanz, A. Moser, and M. Braun, "Simbench—a benchmark dataset of electric power systems to compare innovative solutions based on power flow analysis," *Energies*, vol. 13, no. 12, p. 3290, 2020.

[27] R. Mosshammer, K. Diwold, A. Einfalt, J. Schwarz, and B. Zehrfeldt, "Bifrost: A smart city planning and simulation tool," in *Intelligent Human Systems Integration 2019: Proceedings of the 2nd International Conference on Intelligent Human Systems Integration (IHSI 2019): Integrating People and Intelligent Systems, February 7-10, 2019, San Diego, California, USA*. Springer, 2019, pp. 217–222.

[28] "Zentralanstalt für meteorologie und geodynamik zamg, "messstationen zehnminutendaten"," http://data.hub.zamg.ac.at, accessed: 2023-07.

[29] "Meteoblue, "weather api,"," www.meteoblue.com, accessed: 2023-07.

[30] R. Sudhoff, S. Schreck, S. Thiem, and S. Niessen, "Operating Renewable Energy Communities to Reduce Power Peaks in the Distribution Grid: An Analysis on Grid-Friendliness, Different Shares of Participants, and Economic Benefits," *Energies*, vol. 15, no. 15, p. 5468, 2022.

[31] M. Abumohsen, A. Y. Owda, and M. Owda, "Electrical load forecasting using lstm, gru, and rnn algorithms," *Energies*, vol. 16, no. 5, 2023. [Online]. Available: https://www.mdpi.com/1996-1073/16/5/2283

[32] S. Hochreiter and J. Schmidhuber, "Long short-term memory," *Neural Comput.*, vol. 9, no. 8, p. 1735–1780, nov 1997. [Online]. Available: https://doi.org/10.1162/neco.1997.9.8.1735

[33] D. P. Kingma and J. Ba, "Adam: A method for stochastic optimization," in *3rd International Conference on Learning Representations, ICLR 2015, San Diego, CA, USA, May 7-9, 2015, Conference Track Proceedings*, Y. Bengio and Y. LeCun, Eds., 2015. [Online]. Available: http://arxiv.org/abs/1412.6980

[34] I. Loshchilov and F. Hutter, "SGDR: stochastic gradient descent with warm restarts," in *5th International Conference on Learning Representations, ICLR 2017, Toulon, France, April 24-26, 2017, Conference Track Proceedings*. OpenReview.net, 2017. [Online]. Available: https://openreview.net/forum?id=Skq89Scxx